Article:
Tummala, N., Reardon, G., Dandu, B. et al. (2026) Biomechanical filtering supports efficient tactile encoding in the human hand. Journal of the Royal Society Interface, 23 (237). 20250793. ISSN: 1742-5689

https://doi.org/10.1098/rsif.2025.0793

INTERFACE

royalsocietypublishing.org/journal/rsif

Research

Cite this article: Tummala N, Reardon G, Dandu B, Shao Y, Saal HP, Visell Y. 2026 Biomechanical filtering supports efficient tactile encoding in the human hand. *J. R. Soc. Interface* **23**: 20250793.
https://doi.org/10.1098/rsif.2025.0793

Received: 31 July 2025
Accepted: 14 January 2026

Subject Category:
Life Sciences–Engineering interface

Subject Areas:
biomechanics, neuroscience

Keywords:
skin mechanics, somatosensory processing, tactile afferents

Author for correspondence:
Yon Visell
e-mail: yonvisell@ucsb.edu

Electronic supplementary material is available online at https://doi.org/10.6084/m9.figshare.c.8342004.

THE ROYAL SOCIETY PUBLISHING

Biomechanical filtering supports efficient tactile encoding in the human hand

Neeli Tummala[1], Gregory Reardon[2], Bharat Dandu[1], Yitian Shao[1], Hannes P. Saal[4] and Yon Visell[3]

[1]Department of Electrical and Computer Engineering, [2]Media Arts and Technology Program, and [3]Department of Mechanical Engineering, University of California Santa Barbara, Santa Barbara, CA, USA
[4]School of Psychology, University of Sheffield, Sheffield, UK

NT, 0009-0004-2133-6029; HPS, 0000-0002-7544-0196; YV, 0000-0003-2742-9256

Touching an object elicits skin oscillations that are biomechanically transmitted throughout the hand, driving responses in thousands of tactile receptors, including numerous exquisitely sensitive Pacinian corpuscles (PCs). Accepted descriptions of PC functionality characterize their response properties as highly stereotyped, based on experimental data gathered when stimuli are applied near the receptor. However, during natural touch, spiking activity in the majority of PCs is evoked by transmitted skin oscillations that are modified by biomechanical filtering. This filtering mechanism, stemming from dispersive wave dynamics in the skin, bears some similarity to the pre-neuronal filtering of auditory signals by the basilar membrane, a mechanical process that is instrumental to perception. Thus, we sought to clarify how skin biomechanics might influence tactile information encoding in the periphery. We used vibrometry imaging and computational neural experiments to examine the influence of biomechanical filtering on neural activity in whole-hand PC populations. We observed complex, location- and frequency-dependent patterns of filtering that were shaped by tissue mechanics and hand morphology. This source of biomechanical modulation diversified PC population spiking activity and enhanced tactile information encoding efficiency. These findings indicate that biomechanics furnishes a pre-neuronal mechanism that facilitates efficient tactile encoding and processing.

1. Introduction

The sense of touch is stimulated when the skin comes into contact with the environment. During such contact events, perceptual information is often regarded as originating from the responses of tactile sensory neurons terminating near the contact location (CL). But the sense of touch is also invoked when the environment is explored indirectly through a probe, such as a tool, fingernail or whisker. Such probes are not innervated by sensory neurons. Instead, perceptual information is mediated by 'internal contacts' that biomechanically couple the probe to skin innervated by tactile sensory neurons [1]. The same biomechanical couplings that mediate indirect touch are also involved during direct touch. In both cases, these couplings facilitate the transmission of touch-elicited skin oscillations to regions far from the CL [2,3], which excites remote tactile sensory neurons [4].

Indeed, manual touch interactions, such as texture exploration [5,6], dexterous manipulation [7] and tool use [8], generate prominent skin oscillations that are transmitted across the hand. The biomechanics of the hand transforms localized contact forces into spatially distributed skin oscillations that carry information about contact at the skin surface [6,9,10]. These oscillations excite widespread Pacinian corpuscle (PC) neurons that encode the transmitted tactile information via spiking responses conveyed to the brain [3,11–13].

Central somatosensory processing integrates tactile inputs from receptors across the hand, reflecting a topographically complex somatotopic organization [14,15]. The central integration of widespread peripheral neural activity is, unsurprisingly, reflected in touch perception. For example, humans can discriminate between different surface textures [16] or vibration frequencies [17] applied to an anesthetized finger, utilizing information encoded by remote PCs. The perceptual significance of PC responses evoked across the hand is also exemplified by tactile summation, masking and transfer learning effects observed when stimuli are applied at separate hand locations [18–20]. Across species, PCs also respond readily to subtle vibrations transmitted through the ground or other substrates, resulting from distant contact events [21–24]. This sensitivity enhances the ability of several species to detect vibrations that facilitate perception and communication over substantial distances [23,24]. In addition, PCs facilitate the perception of contact events during object manipulation and tool use, highlighting their integral role in both direct and mediated tactile perception [7,8,25].

Recent studies suggest that hand biomechanics modifies transmitted skin oscillations through frequency-dependent and location-specific filtering imparted by tissues [11,26], which may increase the stimulus information content available to tactile sensory neurons [27]. However, the specific effects of biomechanical filtering on PC spiking activity throughout the hand are unknown. Existing peripheral neural recordings reveal PC response characteristics to be highly stereotyped, with the highest frequency sensitivity between 200 and 300 Hz [28–32]. However, these recordings are only obtained from PCs closest to the stimulus CL. As a result, they do not capture the effects of biomechanical filtering, which predominantly influence the responses of distant PCs. Thus, the influence of biomechanical filtering on tactile encoding by whole-hand PC populations and its implications for tactile sensing has received little prior attention.

It is not straightforward to deduce biomechanical influences on PC population responses owing to the complex and heterogeneous morphology of the hand. Furthermore, extant experimental techniques preclude the simultaneous recording of neural signals from populations of PCs in the human hand [33]. To overcome these limitations, we captured high-resolution vibrometry measurements of skin oscillations across the whole hand. We then used location-specific vibrometry measurements to selectively drive each receptor in a whole-hand population of spiking PC neuron models. We analysed the vibrometry measurements to determine the frequency- and location-dependent patterns of biomechanical filtering. Using our data-driven neural simulation methodology, we then characterized the location-specific influences of biomechanical filtering on the tuning characteristics of PCs located throughout the hand, and the implications for tactile encoding by whole-hand PC populations. Our findings reveal that biomechanical filtering in the periphery furnishes a pre-neuronal mechanism that modulates and diversifies PC population spiking responses, thereby supporting efficient somatosensory encoding and processing.

2. Results

2.1. Imaging whole-hand biomechanical transmission

We characterized the transmission of skin oscillations across the glabrous skin of several human hands ($n = 7$, P1 to P7). Mechanical impulses (0.5 ms duration) were applied at four distinct CLs, and evoked skin oscillations were recorded at 200 to 350 spatially distributed locations via optical vibrometry (sample rate 20 kHz, grid spacing 8 mm; see §4; figure 1A). These impulse response measurements characterized biomechanical transmission across the hand within the frequency range relevant to PCs (20 to 800 Hz). The dispersive nature of biomechanical transmission altered both the temporal structure (figure 1B) and frequency content (figure 1C) of skin oscillations. As a consequence, we observed the pairwise correlation of skin oscillations at different locations to decrease with increasing pairwise distance (figure 1D).

Using the measured impulse responses, we computed the skin oscillations that would be evoked by arbitrary tactile stimuli by leveraging the linearity of biomechanical transmission in the small-signal regime. Prior work has shown that linearity holds over the frequency and displacement ranges used here [34–36]. Thus, a standard result from linear systems theory applies [37]: the skin oscillations elicited by any tactile stimulus can be obtained by convolving the stimulus waveform with the measured impulse responses (see §4; electronic supplementary material, fig. S1). This method applies the biomechanical filtering encoded by the impulse responses to the stimulus waveform, including any location-dependent modulation of frequency content, amplitude and phase imparted by hand biomechanics. For example, skin oscillations computed for a broadband noise stimulus exhibited distance-dependent patterns of amplitude variation and temporal correlation similar to those observed in the impulse response measurements (figure 1E,F). We verified the accuracy of this method by showing that the skin oscillations obtained by convolution closely matched those we directly measured for a set of stimuli encompassing a wide range of frequencies (electronic supplementary material, figs. S2 and S3). This approach enabled us to compute skin oscillations evoked by a large variety of stimuli, including sinusoids, diharmonics and bandpass-filtered noise, which would be impractical to measure directly. We then used the computed skin oscillations as inputs to an ensemble of PC neuron models to simulate spiking activity in a population of PCs distributed across the hand (see §4; electronic supplementary material, fig. S1).

2.2. Biomechanically mediated PC spiking activity

PC spiking responses are driven by deformations of the corpuscle caused by mechanical oscillations of surrounding tissues [32]. Thus, we sought to characterize the influence of biomechanical filtering on PC spiking responses. However, current experimental techniques preclude the *in vivo* measurement of PC population responses in the human hand [33]. To overcome this limitation, we determined the spiking responses of whole-hand PC populations for arbitrary tactile stimuli *in silico*. We used skin oscillations

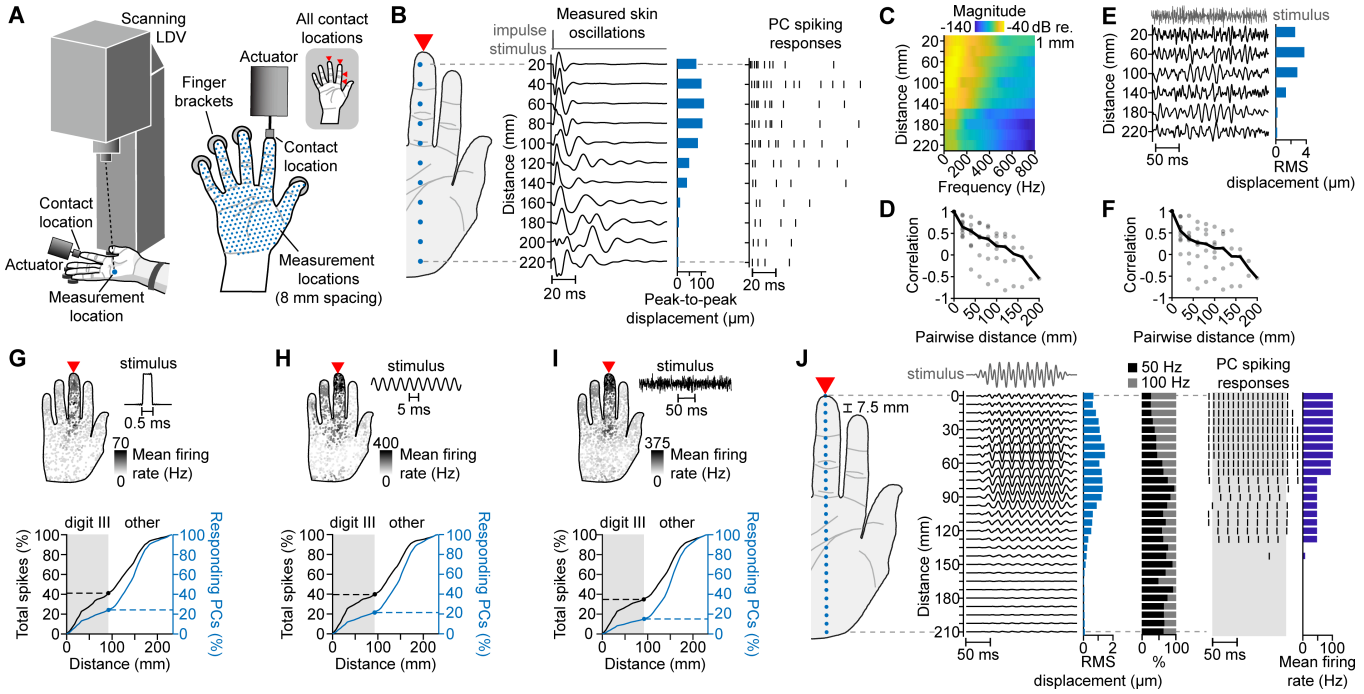

Figure 1. Evoked skin oscillations drive location-specific spiking responses in PCs throughout the hand. (A) An impulse was applied at one of four CLs, and the resulting skin oscillations (i.e. impulse responses) were measured at more than 200 locations across the hands of seven participants using a scanning laser Doppler vibrometer (SLDV). (B) Left: impulse responses measured at a subset of measurement locations (blue dots). Red arrow indicates CL. Right: PC spiking responses evoked by the respective measured impulse responses, shown for PC neuron model type 4. Subfigures (B–J) show data from Participant 5 (P5). (C) Magnitude spectra of the measured impulse responses in (B). The frequency content of the impulse responses varies with distance from the CL. (D) Correlations between the measured impulse responses in (B) decrease as distance between the measurement locations increases. Grey dots: Pearson correlation coefficients computed between the full time-domain waveforms of each pair of impulse responses in (B); black line: median correlation at each pairwise distance. (E) Skin oscillations computed for a bandpass-filtered noise stimulus (top trace, 50 to 800 Hz band) applied at the digit III distal phalanx (DP). (F) Correlations between the computed skin oscillations shown in (E) exhibit a similar distance-dependent decrease to those observed for the impulse responses in (D). Grey dots: Pearson correlation coefficients computed between the full time-domain waveforms of each pair of computed skin oscillations in (E); black line: median correlation at each pairwise distance. (G) Upper panel: PC mean firing rates evoked by measured skin oscillations that were elicited by an impulse applied at the digit III DP (red arrow; 15 μm max. peak-to-peak displacement across hand). Lower panel: cumulative percentage of spikes (black) and responding PCs (blue) located within increasing distances from the CL. Shaded region: results within digit III. The majority of evoked neural activity, whether assessed as total number of spikes or number of responding PCs, occurs outside of the stimulated digit. (H) As in (G), but evoked by skin oscillations computed for a 200 Hz sinusoidal stimulus (15 μm max. peak-to-peak displacement across hand). (I) As in (G), but evoked by skin oscillations computed for a bandpass-filtered noise stimulus (50 to 800 Hz band, 5 μm max. RMS displacement across hand). (J) PC spiking responses (right, PC neuron model type 4) evoked by skin oscillations (middle) at selected locations (left, blue dots) computed for a diharmonic stimulus ($f_1 = 50$ Hz, $f_2 = 100$ Hz) applied at the digit III DP (red arrow). Light blue bars: root mean square (RMS) displacements of skin oscillations; black and grey bars: percentage of skin oscillation magnitude spectrum composed of 50 Hz (black) or 100 Hz (grey) components; dark blue bars: PC firing rates calculated from spikes within shaded region. PCs located at different distances from the CL respond to different frequency components of the stimulus.

computed from the measured impulse responses to drive a population of spiking PC neuron models that were fit to physiological data in prior research [38] (electronic supplementary material, fig. S1). Each PC neuron model was driven by skin oscillations computed at its location in the hand. The neuron models were randomly assigned one of four types, each trained on data from a different PC, thereby capturing intrinsic variability in PC response properties arising from factors such as receptor size and shape (electronic supplementary material, fig. S8A). The spatial distribution of PCs across the hand was selected based on findings from a prior anatomical study [39]. We used this methodology to obtain whole-hand PC population spiking responses evoked by arbitrary tactile inputs supplied at any of four CLs on the hand.

All stimuli evoked spiking activity in PCs throughout the hand, consistent with predictions from theory and findings from prior studies [3,6,11]. The majority of the elicited spiking activity and responding PCs were in hand regions far removed from the CL. This was true for all stimulus types, including brief impulses (figure 1G), sinusoids (figure 1H and electronic supplementary material, fig. S4A,B) and bandpass-filtered noise stimuli (figure 1I and electronic supplementary material, fig. S4C,D). In each case, the magnitude and timing of PC spiking activity were directly modulated by location-specific changes in the frequency content, amplitude and phase of the skin oscillations. For example, a brief impulse evoked PC spiking responses that varied based on hand location and exhibited sustained firing for more than 20 ms owing to temporal spreading in the measured skin oscillations, which arises from dispersive wave propagation in the skin (figure 1B) [26,40].

PC responses also exhibited characteristic entrainment behaviour (phase-locking to the oscillations of periodic stimuli) that was modified by biomechanical filtering. For example, a diharmonic stimulus applied at the fingertip evoked distance-dependent patterns of entrainment (figure 1J): receptors near the CL (less than 60 mm) entrained to the higher frequency signal component (100 Hz), while more distant receptors entrained to the lower frequency component (50 Hz). This distance-dependent entrainment behaviour arose owing to the greater attenuation of higher frequency skin oscillations with distance (figure 1J, black and grey bars),

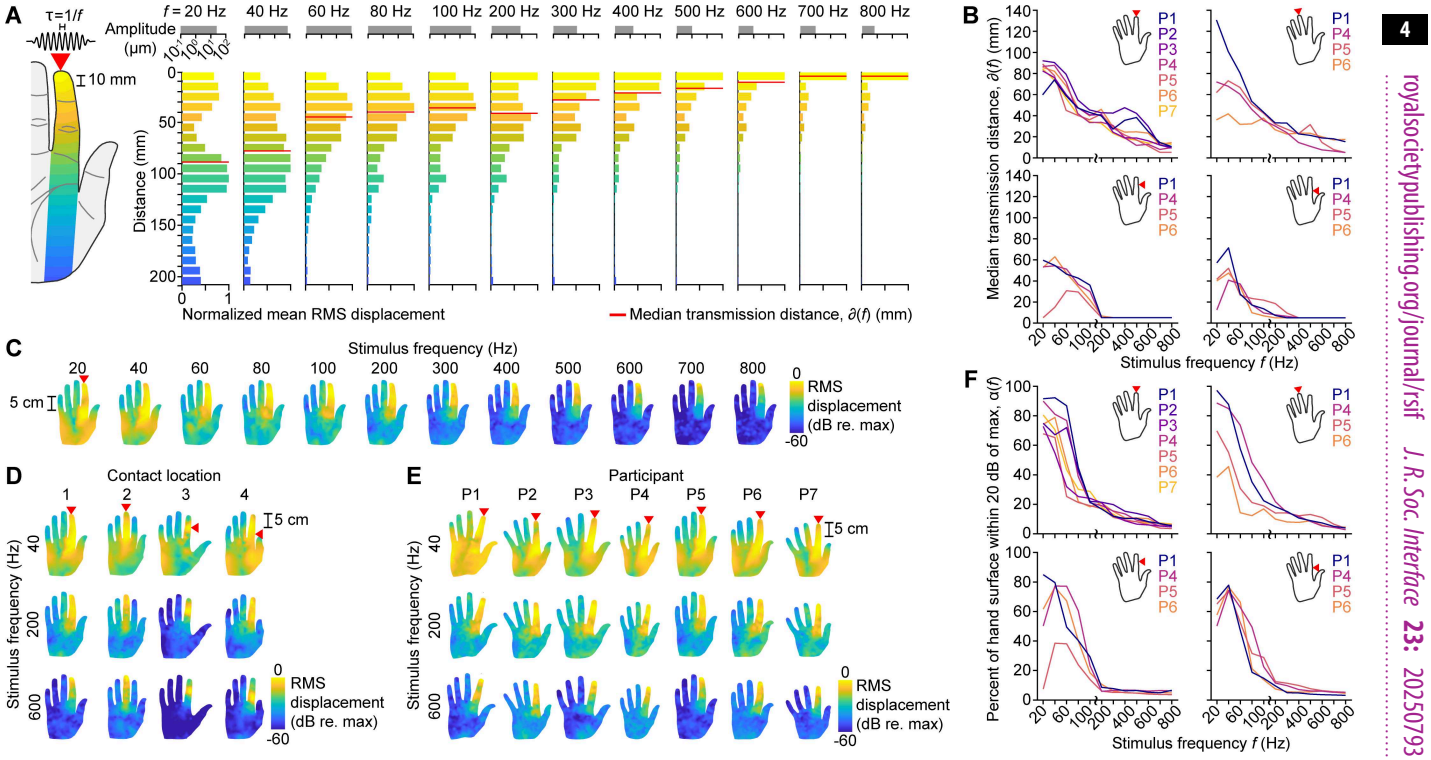

Figure 2. Biomechanical filtering in the hand is frequency- and location-dependent. (A) Normalized RMS skin displacements averaged within 10 mm wide bands at increasing distances from the CL computed for sinusoidal stimuli of various frequencies (20 to 800 Hz). The oscillation amplitudes vary greatly with stimulus frequency and skin location. Scale bars (top, grey) show maximum peak-to-peak displacement across the hand at each frequency. Red lines: median transmission distance $\partial(f)$; red arrow: CL. Shown for P5. (B) Median transmission distance, $\partial(f)$, of RMS skin displacement distributions as a function of stimulus frequency f, for all participants (lines) and CLs (panels). Lower frequency stimuli evoke skin oscillations that are transmitted farther across the hand. Red arrows: CL; line colour: participant. (C) RMS displacement across the hand computed for sinusoidal stimuli of various frequencies (20 to 800 Hz). Spatial patterns of skin oscillations vary greatly with stimulus frequency. Red arrow: CL. Shown for P5. (D) As in (C), for other CLs. Shown for P5. (E) As in (C), for P1 to P7. (F) Percentage of hand surface, $\alpha(f)$, where RMS skin displacement is within 20 dB of the maximum RMS displacement as a function of stimulus frequency f, for all participants (line colours) and CLs (panels). Lower frequency stimuli evoke prominent skin oscillations over larger areas of the hand. Red arrows: CL; line colour: participant. Analyses in (A–F) used skin oscillations computed from the measured impulse responses.

an effect of tissue viscoelasticity [2,26]. Thus, PCs at different locations in the hand encode different frequency components of the same stimulus.

2.3. Location-specific biomechanical filtering

To more fully characterize biomechanical filtering, we analysed how it varied with stimulus frequency by computing skin oscillations across the whole hand for sinusoidal stimuli ranging from 20 to 800 Hz. The computed skin oscillations exhibited distance-dependent amplitudes that varied greatly with stimulus frequency (figure 2A; results for other participants and CLs: see electronic supplementary material, fig. S5). To quantify these frequency-dependent differences, we defined the median transmission distance $\partial(f)$ as the weighted median of distance from the CL, with weights given by the oscillation amplitudes evoked by stimulus frequency f (figure 2B). At low frequencies ($f \leq 100$ Hz), $\partial(f)$ extended well beyond the stimulated digit (mean $\partial(f)$ across participants = 49.7 mm), and the amplitude decay was non-monotonic with distance from the CL. By contrast, at high frequencies ($f > 100$ Hz), skin oscillations were concentrated within the stimulated digit (mean $\partial(f)$ across participants = 14.8 mm) and exhibited relatively monotonic decay with distance. These complex, frequency-dependent patterns of biomechanical filtering are a function of soft tissue viscoelasticity and the heterogeneous morphology of the hand. We observed a larger $\partial(f)$ at low frequencies and smaller $\partial(f)$ at high frequencies for all participants and CLs, with a larger range of $\partial(f)$ across participants at low frequencies (mean range = 30.6 mm for $f \leq 100$ Hz versus 8.3 mm for $f > 100$ Hz).

We further observed the influences of morphology and skeletal structure in the spatial patterns of biomechanical filtering across the whole hand (figure 2C–E; results for all participants and CLs: electronic supplementary material, fig. S6). At low frequencies ($f \leq 100$ Hz), transmission was notably enhanced near the metacarpophalangeal (MCP) joint of the stimulated digit and in the lateral and contralateral extensions of the palmar surface (thenar and hypothenar eminences) for all participants (electronic supplementary material, figs. S6 and S7). To quantify how these whole-hand patterns of skin oscillations varied with stimulus frequency f, we calculated $\alpha(f)$, the percentage of the hand surface where oscillation amplitudes were within 20 dB of the maximum amplitude across the hand (figure 2F). Averaged across participants, $\alpha(f)$ was 50% for $f \leq 100$ Hz compared to 8% for $f > 100$ Hz, consistent with our analysis of $\partial(f)$. Low-frequency stimuli evoked prominent oscillations over a substantially larger fraction of the hand surface than high frequencies for all participants and CLs, with a larger range of $\alpha(f)$ across participants at low frequencies (mean range = 33.5% for $f \leq 100$ Hz versus 4.4% for $f > 100$ Hz).

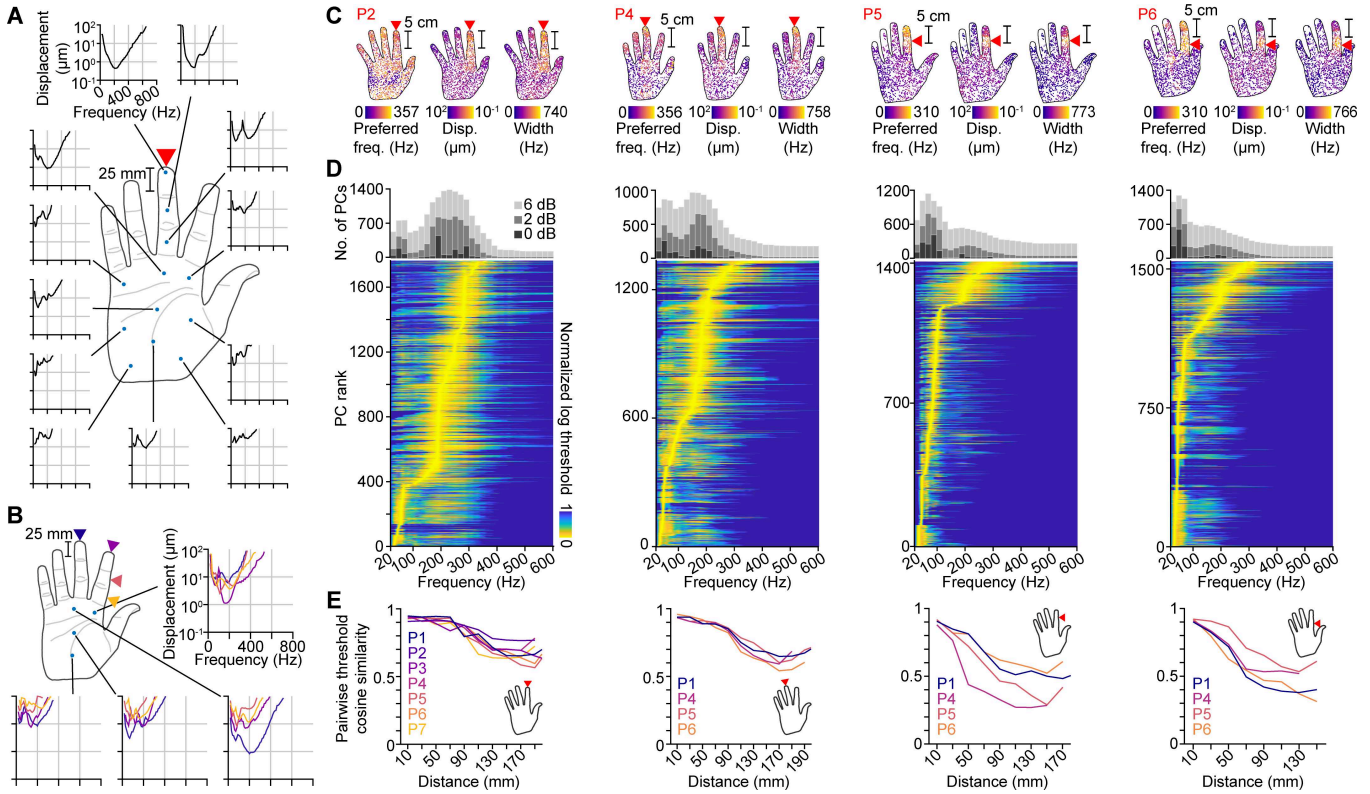

Figure 3. Biomechanical filtering diversifies PC response characteristics. (A) Entrainment threshold curves of PCs at selected locations (blue dots). PCs near the CL have canonical threshold curves, while those farther away exhibit markedly different frequency sensitivities. *x*-axes: stimulus frequency; *y*-axes: minimum stimulus displacement needed to evoke entrainment; red arrow: CL. Shown for PC neuron model type 4 and P1. (B) Entrainment threshold curves of PCs at selected locations (blue dots) for each of four CLs (coloured arrows), showing that the threshold curve of a given PC varies with CL. Line colours correspond to CLs. Shown for PC neuron model type 4 and P1. (C) Preferred frequency (left), minimum curve value (middle), and curve width (right) for each PC in the hand. PC populations exhibit substantial variability in all three properties. Red arrow: CL; red text: participant number. (D) Lower panel: Entrainment threshold curves for all PCs in the hand rank ordered by preferred frequency. Upper panel: Number of PCs at each frequency with entrainment threshold curve values within 0 dB (light grey), +2 dB (medium grey) and +6 dB (dark grey) of the curve minimum. A large proportion of the PC population exhibits preferred frequencies outside of the canonical range (200–300 Hz). Participants and CLs as in (C). (E) Median cosine similarity between all pairs of entrainment threshold curves of PCs located within 10 mm of the CL and those of PCs located within 20 mm wide bands at increasing distances from the CL. Similarity decreases with distance from the CL, highlighting the diversity of threshold curves across the hand. Centre distance for each band shown on *x*-axis. Shown for all participants (lines) and CLs (panels). Red arrows: CL; line colour: participant. Analyses in (A–E) used skin oscillations computed from the measured impulse responses.

2.4. Biomechanical filtering modulates PC tuning

We next examined how biomechanical filtering modulates the tuning characteristics of PCs, as reflected in their frequency-dependent entrainment behaviour (figure 1J). To do this, we analysed whole-hand PC spiking activity evoked by sinusoidal stimuli with different frequencies (20 to 800 Hz). We characterized the frequency-dependent sensitivity of PCs by computing entrainment threshold curves, which represent the minimum stimulus displacement required to evoke entrainment at each frequency (see §4). PCs located near the CL exhibited U-shaped entrainment threshold curves with preferred (most sensitive) frequencies between 200 and 300 Hz (figure 3A and electronic supplementary material, fig. S8A). This result is consistent with established descriptions of PC function, which are based on *in vivo* experiments where the stimulus is applied adjacent to the PC [28–32]. However, we obtained diverging findings for the larger number of PCs located outside the contact region. Entrainment threshold curves for remote PCs varied greatly and exhibited multiple prominent minima for all participants and CLs, reflecting location-specific effects of biomechanical filtering (figure 3A and electronic supplementary material, fig. S8B,C). Throughout the hand, threshold curves varied in a complex, non-monotonic manner with receptor location. Threshold curves also varied with the stimulus CL (figure 3B).

We further analysed the distribution of frequency tuning across whole-hand PC populations by rank ordering all entrainment threshold curves by preferred frequency (figure 3C,D; results for all participants and CLs: see electronic supplementary material, fig. S9). Within each population, PCs exhibited diverse preferred frequencies, ranging from 24 to 420 Hz (electronic supplementary material, fig. S10A–D). Across participants, minimum preferred frequencies ranged from 24 to 30 Hz, and maximum preferred frequencies ranged from 310 to 420 Hz. The preferred frequencies of PCs located near the CL were consistent with values obtained in prior studies (200 to 300 Hz), as noted above. However, PCs located outside the contact region exhibited a wider range of frequency sensitivities (electronic supplementary material, fig. S10E–H). Strikingly, across all participants and CLs, a substantial proportion of PCs in a population preferred frequencies below 100 Hz (mean 47%). Only a minority of PCs in the hand (less than 20%) had preferred frequencies between 200 and 300 Hz. PCs at greater distances from the CL exhibited more narrowly tuned curves and higher thresholds, indicating greater specificity in frequency preference and lower sensitivity (figure 3C).

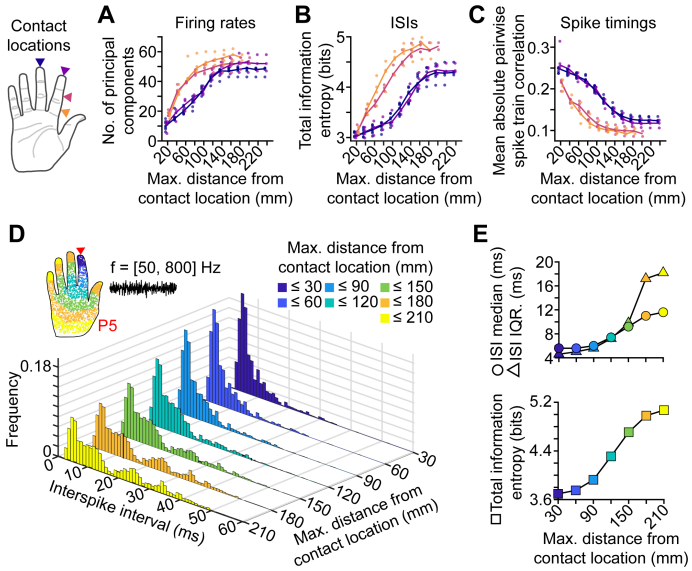

Figure 4. Biomechanical filtering diversifies PC spiking activity. (A) Number of principal components explaining 99% of the variance in the firing rates of PCs within increasing distance ranges from the CL. Latent dimensionality of the firing rates increases with distance from the CL. Colours indicate CL; dots: data points for each participant; lines: median across participants. Analyses in (A–C) are conducted on PC spiking activity evoked by a diverse stimulus set. (B) Total information entropy of interspike interval (ISI) distributions (1 ms bin width) constructed from the spiking activity of PCs within increasing distance ranges from the CL. Entropy increases with distance, indicating that PCs farther from the CL increase the diversity of spike-timing patterns present in the population. Plot can be read as in (A). (C) Mean absolute spike train correlation between all pairs of PCs both located within increasing distances from the CL. Spike train correlations decrease with distance, demonstrating that PCs farther from the CL contribute distinct responses to the population activity. Spike trains were binned with a bin width of 1 ms. Plot can be read as in (A). (D) ISI histograms constructed from the spiking activity of PCs located within increasing distances from the CL (hand inset) in response to a bandpass-filtered noise stimulus (50 to 800 Hz band, 5 µm max. RMS displacement across hand, 175 ms duration) applied at the digit II DP of P5. (E) Median (circles), interquartile range (triangles), and total information entropy (squares) of the ISI histograms shown in (D). All three statistics increase with distance, showing that PCs farther from the CL exhibit a wider range of ISIs. Analyses in (A–E) used skin oscillations computed from the measured impulse responses.

However, the entrainment threshold curves exhibited complex shapes that varied greatly with hand location in a manner not adequately summarized by preferred frequency, curve width or minimum threshold. To characterize distance-dependent variations in the threshold curves, we instead calculated the pairwise cosine similarity between threshold curves of PCs at the CL and those within regions at progressively greater distances from the CL (figure 3E; results for all participants and CLs: electronic supplementary material, fig. S11). For all participants and CLs, the median cosine similarity between threshold curves decreased with increasing distance from the CL (0.021 to 0.086 per 20 mm; $R^2 = 0.76$ to 0.94). Thus, threshold curves became more distinct as distance from the CL increased.

2.5. Biomechanical filtering diversifies tactile encoding

We next asked whether this diversification enhanced information encoding in PC population spiking responses, particularly for the large proportion of PCs outside the contact region. To address this, we characterized the dimensionality and information content of PC population spiking activity as a function of distance from the CL. Informed by prior research [41,42], we employed a diverse set of stimuli containing sinusoidal, diharmonic and bandpass-filtered noise signals with various frequency and amplitude parameters (electronic supplementary material, tables S1–S3). We used principal component analysis (PCA) to assess the latent dimensionality of PC firing rates in subpopulations of PCs within increasing maximum distances from the CL. For all participants and CLs, dimensionality, calculated as the number of principal components needed to capture 99% of the variance in the firing rates, increased with distance (figure 4A; mean range across participants = 7.3 principal components). Latent dimensionality was two to five times higher for subpopulations within maximum distances of 100 mm or more from the CL than it was for subpopulations within distances of 20 mm or less. Thus, PCs at increasing distances contributed additional variability in firing rates that was not captured by PCs at the CL.

In addition to firing rates, PCs signal information about touch events via spike timing [42]. We characterized information encoded in PC spike timing by computing the Shannon information entropy of interspike interval (ISI) histograms constructed from the spiking activity of PC subpopulations within increasing maximum distances from the CL. For all stimuli, ISIs were generally larger and more broadly distributed with increasing distance (figure 4D,E and electronic supplementary material, fig. S12). Consequently, information encoded in the ISIs increased monotonically with distance by a factor of more than 1.4 before plateauing at distances of 140 to 180 mm from the CL for all participants and CLs (figure 4B; mean range across participants = 0.27 bits). The findings were robust to variations in ISI histogram bin widths (electronic supplementary material, fig. S13A–G).

We also analysed the correlations between spiking responses evoked in subpopulations of PCs within increasing maximum distances from the CL. Consistent with the ISI findings, as distance increased, the spiking responses of remote PCs became progressively less correlated with the spiking responses of PCs near the CL for all participants and CLs, as quantified by mean pairwise

spike train correlations (figure 4C; mean range across participants = 0.02; see electronic supplementary material, fig. S13H–N for variations in bin width). Together, these information encoding measures demonstrate that biomechanical filtering diversifies PC spiking activity by enabling remote PCs to encode information not captured by PCs near the CL, thereby supporting tactile encoding efficiency [43,44]. The plateaus in the computed measures also indicate that some response redundancy is preserved within the population responses.

3. Discussion

Our study combines high-resolution vibrometry measurements of whole-hand biomechanical transmission with simulations of large PC populations based on physiologically validated neuron models [38]. Using this measurement-driven approach, we show that low-frequency components of touch-evoked skin oscillations propagate over large regions of the hand, whereas high-frequency components remain confined near the CL (figure 2). This frequency- and location-dependent biomechanical filtering is broadly consistent with prior studies of wave propagation in the glabrous skin [11,26,34]. However, our measurements reveal substantially more spatiotemporal structure across the whole hand, including non-monotonic decay of oscillation amplitude with distance, influences of hand anatomy on transmission, and CL-dependent variations in filtering. These striking effects of whole-hand biomechanical filtering have not been previously characterized, despite prior literature recognizing that biomechanical transmission is integral to the PC sensory channel [3,11–13].

By integrating our measurements with neural simulations, we reveal that biomechanical filtering plays a prominent pre-neuronal role in modulating and diversifying PC population responses. The canonical PC response characteristics obtained when stimulation is applied near individual receptors, including U-shaped entrainment threshold curves with minima between 200 and 300 Hz [28–32], do not hold for the majority of PCs in the hand that are excited by a tactile stimulus. Rather, PCs away from the CL exhibit diverse threshold curves with a wide range of preferred frequencies, bandwidths and thresholds (figure 3). These remote PCs dominate the total population response during touch events (figure 1G–I) and can thus be expected to affect downstream tactile processing and, ultimately, perception.

Several prior psychophysics and perception studies suggest that the widespread PC activity we reveal here is perceptually significant. Vibrotactile summation and masking effects arise between stimuli applied at distant hand locations, indicating that signals captured by widely distributed PCs are integrated in downstream processing [18,19]. The perceptual influence of activity in PCs remote from the CL is also evident in individuals with impaired tactile sensation owing to anaesthesia, nerve compression or traumatic injury: they are able to detect and discriminate vibrations applied to areas of the hand lacking sensation through remote PC activity evoked by biomechanical transmission [17,45,46]. Similarly, fine surface textures explored with an anesthetized finger can be perceptually discriminated owing to the responses of remote PCs excited by transmitted skin oscillations [6,16]. The influence of biomechanically mediated PC activity on tactile perception also extends to artificial haptic feedback. For example, the inverse relationship between stimulus frequency and transmission distance (figure 1B,F) has been exploited to generate frequency-controlled haptic effects that are felt to expand or contract from a single localized stimulation site [26]. Biomechanical transmission was also found to strongly influence the perception of tactile motion applied with airborne ultrasound [47].

Our finding that biomechanical filtering gives rise to diverse PC response characteristics across the hand may provide insight into how PC populations encode stimuli with varying or complex frequency content. This, in turn, may shed light on aspects of human tactile perception that are not yet fully understood. For example, perceived intensity exhibits a dependence on stimulus frequency that cannot be fully explained by predictions derived solely from the responses of PCs adjacent to the stimulation site [41,48,49]. Our findings suggest that accounting for PCs farther from the CL, which exhibit diverse response characteristics (figure 3) and distinct spiking activity (figure 4), may help resolve this discrepancy. These findings can also be applied to understanding how PC populations encode stimuli with complex frequency content. The biomechanical modulation of PC frequency sensitivity that we observe bears some resemblance to the frequency-place transform of the mammalian cochlea, where subpopulations of auditory neurons exhibit distinct frequency tuning as a consequence of inner ear biomechanics [50,51]. Prior psychophysics studies drew inspiration from this aspect of peripheral auditory encoding to propose models for the tactile perception of stimuli with complex frequency spectra [52,53]. These studies found that human abilities of frequency discrimination were well-explained by models in which a stimulus activates a set of functional ‘mini-channels’, each containing receptors tuned to a distinct frequency. Although these models failed to gain traction owing to a lack of evidence for such receptor subpopulations, our findings provide a mechanistic rationale that may motivate further investigation. Specifically, we find that PCs at different locations in the hand respond to different frequency components of broadband or polyharmonic stimuli owing to location-dependent filtering of skin oscillations imparted by hand biomechanics (figure 1J). This suggests that psychophysical measures of vibrotactile intensity and frequency discrimination arise from the integration of PC activity across the whole hand, rather than at the contact site alone. Further research is needed to investigate these perceptual implications, including for complex naturalistic stimuli evoked during texture exploration and object manipulation [7,9].

Our findings may also shed light on a number of peculiar aspects of PC innervation of the hand. At the level of peripheral encoding, PCs exhibit stereotyped response properties [28–32], large receptive fields that span most of the hand [54] and high densities in the glabrous skin [39,55–57]. Taken in isolation, these features would imply significant redundancy in PC population responses. However, our results demonstrate that biomechanical filtering diversifies PC response characteristics and spiking activity, thereby reducing population response redundancy and enhancing encoding efficiency. These findings align with predictions from recent modelling work [27]. At the anatomical level, our findings suggest a functional rationale for the prominent clustering of PCs near the MCP joints [56,57]. We found that skin oscillations evoked by low-frequency stimuli (less than 100 Hz)

were amplified near the MCP joint of the stimulated digit (figure 2C–E, electronic supplementary material, fig. S7), indicating that these may be advantageous locations for PCs.

Despite the observed complexity of biomechanical transmission in the hand, several characteristics were conserved across multiple hands and CLs. Across all conditions, oscillation amplitudes varied with distance in a frequency-dependent manner and low frequencies were transmitted over longer distances and larger areas of the hand surface (figure 2B,F). Moreover, in the majority of conditions, oscillations were amplified near the MCP joints of the stimulated digit and along the thenar and hypothenar regions of the palm (electronic supplementary material, figs. S6 and S7). Together, these regularities suggest that biomechanical filtering imposes a spatial-spectral structure on touch-evoked signals that the brain could learn and exploit, in apparent agreement with hypotheses for efficient encoding of whole-hand touch events [58], object slippage [59] and tool use [8].

In addition to these conserved features, we observed variability in biomechanical transmission across participants, particularly at low frequencies. This probably arose from differences in hand posture and contact condition [60], hand size and anatomy and tissue properties such as hydration and stiffness [61]. Investigating how these factors shape biomechanical transmission, and in turn PC population responses, is an important avenue for future work, with implications for understanding the extent to which perceptual processing is influenced by biomechanical and anatomical variations.

4. Methods

4.1. *In vivo* optical vibrometry

Mechanical oscillations across the volar hand surface were imaged with a scanning laser Doppler vibrometer (SLDV; model PSV-500, Polytec, Inc., Irvine, CA; sample frequency 20 kHz) fastened to a pneumatically isolated table. During each recording, the hand was fixed to the table in an open, palm-up posture via custom-fit three-dimensional-printed supports that were fastened to the table and adhered to the fingernails of all but the stimulated digit (figure 1A). The LDV, actuator and participants' arms were supported on an optical table equipped with a pneumatic vibration isolation system (Thorlabs T48WK Nexus), which minimized vibration transmission from the environment. The table's large mass (632 kg), thickness (300 mm) and stiffness also impeded vibration transmission through the table. Participants ($n = 7$, 5 male) were 20 to 45 years of age (mean 27.4 years) and were recruited from the student and staff population at the authors' institution. The sample size was determined based on previously published research employing similar methodologies [10,11,26,58]. Participants were seated in a reclined chair with the arm relaxed, supported by a foam armrest, and constrained with Velcro straps. All participants gave their informed, written consent prior to the data collection. The study was approved by the Human Subjects Committee of the University of California, Santa Barbara (Protocol Number 9-18-0676).

The SLDV imaged spatially and temporally resolved skin oscillations at sampling locations distributed on a uniform grid covering the entire volar hand surface (grid spacing 8 mm, 200 to 350 locations). The sampling grid exceeded the Nyquist criterion threshold for frequencies in the tactile range (0 to 1000 Hz), at which spatial wavelengths are between 20 and 100 mm [58]. Oscillations were imaged in the normal direction to the skin surface. Prior vibrometry measurements have demonstrated that most of the energy in evoked skin oscillations is concentrated in oscillations normal to the skin surface [26] and that stress in the normal direction is highly predictive of PC spiking responses [38].

All data were captured from the right hands of participants. Hand lengths ranged from 18 to 21.6 cm (mean 19.9 cm) as measured from the tip of digit III to the bottom of the hand at the middle of the wrist. Each hand was positioned 36 mm below the SLDV aperture, which ensured that the measurements captured at least 95% of the signal variance at all measurement locations. Each participant's hand shape and the two-dimensional (2D) spatial coordinates of all measurement locations were captured via the integrated SLDV geometry processor and camera. Measurements were interpolated to obtain skin oscillations at other locations on the 2D hand surface (see electronic supplementary material).

Measured skin oscillations were evoked by mechanical impulses (rectangular pulse, duration 0.5 ms) applied at each of the four CLs described below. Measurements were synchronized to the stimulus onset. Each measurement was obtained as the median of 10 captures and bandpass filtered to the vibrotactile frequency range (20 to 1000 Hz). Obtaining the median of multiple captures improved signal-to-noise ratio and reduced the effect of spurious data points. The number of captures was selected to balance experimental time and noise reduction. Variability between the captures was modest. For each measurement location, we computed the Pearson correlation coefficient and the mean absolute deviation between each individual capture and the median of the captures. Across measurement locations, the median Pearson correlation coefficient was more than 0.99 and the median normalized mean absolute deviation was less than 2% for all participants and CLs (electronic supplementary material, fig. S14). Frequency analysis was performed by computing magnitude spectra, which were smoothed using a moving median window (width: three samples) to remove measurement artefacts. Numerical frequency-domain integration was employed to obtain skin displacement from velocity.

Stimuli were delivered via an electrodynamic actuator (Type 4810, Brüel & Kjær) driven with a laboratory amplifier (PA-138, Labworks). The actuator terminated in a plastic probe (7×7 mm contact surface) that was adhesively attached to the skin at the stimulus CL. Participants were trained to maintain a preload of 1–2 N between the actuator probe and the skin. The actuator and probe were configured to avoid obstructing the optical path used for the SLDV measurements. The actuator was voltage controlled and its frequency response in acceleration was approximately flat across the range of frequencies used here (20–1000 Hz), as documented in the manufacturer datasheet and confirmed with accelerometer measurements. The electrical impedance of the actuator was also constant within the same frequency range. Therefore, the input voltage and output force of the actuator were

related by a constant factor. We measured this factor using a force transducer (Nano17, ATI Industrial Automation) and determined that the force amplitudes produced by the actuator averaged approximately 0.25 N, with values ranging from 0.2 to 0.4 N. We adjusted the force amplitude within this range to maintain an adequate signal-to-noise ratio in the LDV measurements and to ensure participant comfort. These specific force amplitudes did not constrain our results because our method for computing skin oscillations exploits the linearity of biomechanical transmission to allow arbitrary scaling of the effective stimulus amplitude.

Stimuli were applied at each of four different CLs that were registered to standard anatomical positions on the hand: the distal phalanx (DP) of digit II along the axis of the finger (CL 1, $n = 7$ participants), the DP of digit III along the axis of the finger (CL 2, $n = 4$), the intermediate phalanx of digit II perpendicular to the axis of the finger (CL 3, $n = 4$) and the proximal phalanx of digit II perpendicular to the axis of the finger (CL 4, $n = 4$) (figure 1A). These measurements took approximately 10 min per contact condition per participant. Measurements for CL 2, 3 and 4 were captured from a subset of participants from which measurements for CL 1 were captured (P1, P4, P5 and P6).

4.2. Computing skin oscillations evoked by arbitrary stimuli

Prior studies have demonstrated that biomechanical transmission in the hand is linear for the frequencies and stimulus magnitudes employed here [34–36]. From linear systems theory [37], the impulse response of a linear system fully encodes the system's response to any stimulus, including any modulation of the frequency content, amplitude and phase of the stimulus waveform. Therefore, the system's response to an arbitrary stimulus can be computed by convolving the stimulus waveform with the impulse response. Here, we empirically determined the impulse responses from four CLs on the digits to locations distributed across the whole hand by measuring the whole-hand skin oscillations evoked by an impulse, as detailed above. We describe the stimulus waveform as the actuator input $F(t)$, which is proportional to the force generated by the actuator. Skin displacements $u(\mathbf{x}, t)$ at skin locations $\mathbf{x}$ elicited by a stimulus $F(t)$ applied at location $\mathbf{x}_0$ can be computed as

$$u(\mathbf{x}, t) = g_{\mathbf{x}_0}(\mathbf{x}, t) * F(t), \tag{4.1}$$

where t is time, $*$ denotes convolution in time and $g_{\mathbf{x}_0}(\mathbf{x}, t)$ are the impulse responses encoding the excitation of skin oscillations at locations $\mathbf{x}$ evoked by a unit Dirac impulse applied at $\mathbf{x}_0$ (i.e. the Green's function sampled at locations $\mathbf{x}$ and $\mathbf{x}_0$). We applied equation (4.1) to compute whole-hand skin oscillations for arbitrary stimuli by convolving the stimulus waveforms with the measured impulse responses (electronic supplementary material, fig. S1).

To validate that convolution with the measured impulse responses could be used to accurately compute skin oscillations elicited by arbitrary stimuli, we compared the skin oscillations computed from the measured impulse responses to those that were directly measured for sinusoidal stimuli with frequencies ranging from 20 to 640 Hz (electronic supplementary material, fig. S2). Consistent with linear systems theory, we found that the computed oscillations closely approximated the actual measurements at all frequencies, providing additional empirical validation for our method of computing skin oscillations (electronic supplementary material, fig. S3). Because this linear systems methodology avoids the need for time-intensive experiments, we used it to compute skin oscillations evoked by arbitrary stimuli in the majority of our analyses.

4.2.1. Stimuli

We analysed skin oscillations $u(\mathbf{x}, t)$ evoked by sinusoidal, diharmonic and bandpass-filtered noise stimulus waveforms $F(t)$. These oscillations were computed via convolution with measured impulse responses, as described above. For sinusoidal stimuli, $F(t) = F_0 \sin(2\pi f t)$, where f is frequency and F_0 is the driving amplitude; F_0 was selected to yield skin oscillations with a specific maximum peak-to-peak displacement across all hand locations D_{pp}:

$$D_{pp} = \max_{\mathbf{x}} \left\{ \max_{t} \{u(\mathbf{x}, t)\} - \min_{t} \{u(\mathbf{x}, t)\} \right\}. \tag{4.2}$$

For diharmonic stimuli, $F(t) = F_1 \sin(2\pi f_1 t) + F_2 \sin(2\pi f_2 t)$, with independent driving amplitudes F_1 and F_2 selected to yield specific values of D^1_{pp} and D^2_{pp}, respectively, the maximum peak-to-peak displacements across all hand locations for each sinusoidal component separately equation (4.2). Bandpass-filtered noise stimuli were synthesized using a spectral Gaussian white noise algorithm [62], then bandpass filtered to the desired frequency range. Each bandpass-filtered noise stimulus was generated from the same Gaussian white noise trace, then scaled by a driving amplitude F_0; F_0 was determined by specifying D_{RMS}, the maximum root mean square (RMS) displacement of skin oscillations across all hand locations:

$$D_{RMS} = \max_{\mathbf{x}} \left\{ \sqrt{\frac{1}{N} \sum_{t=1}^{N} u^2(\mathbf{x}, t)} \right\}, \tag{4.3}$$

where N is the number of time samples in each skin oscillation waveform.

4.3. Whole-hand neural simulations

PC population spiking responses were obtained *in silico* by using the computed skin oscillations to drive a population of spiking neuron models extracted from a simulation package (Touchsim [38], Python) (electronic supplementary material, fig. S1), similar to the methodology applied in prior work investigating PC population responses during whole-hand touch events [13]. The PC

neuron models were trained and validated on electrophysiology recordings obtained in a prior study from non-human primates [41]. The models comprised four types, each trained on recordings from a different PC. Consequently, each model type captures the response properties of a unique PC (electronic supplementary material, fig. S8A), reflecting intrinsic variability owing to factors such as receptor size and shape. The PC neuron models supply a nonlinear mapping from skin displacement to spiking output and accurately reproduce experimentally identified PC response characteristics, including response thresholds that vary across several orders of magnitude over the vibrotactile frequency range [29,31] and frequency-dependent thresholds of entrainment [28,30,32]. The stimulus amplitudes used in this work fell within the range over which the PC models were validated.

Whole-hand PC populations were assembled by sampling a random distribution weighted by spatial densities reported in prior studies [39,55]: 25 PCs per cm^2 in the distal phalanges and 10 PCs per cm^2 in the rest of the hand. Except where otherwise noted, the PC neuron model type for each PC in a population was randomly selected to be one of the four types noted above. This assignment captures intrinsic variability across PCs without assuming a particular population-level distribution of PC response properties, since the relative prevalence of such properties is unknown. Each PC was driven by the time-varying skin oscillations $u(\mathbf{x}_m, t)$, where $\mathbf{x}_m$ is the PC location. This produced a spike train represented as an ordered sequence $\mathbf{s}_m = \{t_1, t_2, ..., t_Q\}$, where each t_i denotes the time of the ith spike, with i indicating spike order number, and Q is the total number of spikes. The spike times are strictly ordered ($t_i < t_{i+1}$).

4.4. PC entrainment threshold curves

Entrainment threshold curves were constructed using single-frequency sinusoidal stimuli ranging from 20 to 800 Hz to characterize PC frequency sensitivity. At each frequency, the driving amplitude of the sinusoidal input stimulus was varied to determine the entrainment threshold for each PC in the whole-hand population. The entrainment threshold was identified as the minimum input driving amplitude at which one spike was elicited per cycle of the sinusoidal stimulus. For a given PC, the entrainment threshold depended on the amplitude of the computed skin oscillations at its location for sinusoidal stimuli applied at the CL. For each mth PC and frequency f, the threshold curve $E_m(f)$ recorded the maximum peak-to-peak displacement of skin oscillations evoked across the hand (D_{pp}, equation (4.2)) at the identified entrainment threshold. The maximum D_{pp} across all conditions was 100 µm. In prior literature, threshold curves were determined by placing the stimulating probe near the hotspot of the terminating neuron [28–32] (electronic supplementary material, fig. S8A). Here, however, we analysed threshold curves for all PCs across the hand with the stimulus CL held constant. This preserved the effects of biomechanical transmission and filtering that were not captured in prior approaches. For each PC, the preferred (most sensitive) frequency was computed as $f^* = \arg\min_f\{E_m(f)\}$. To characterize sensitivity bandwidth, the width of each threshold curve was defined as the frequency range in which the curve fell below half-amplitude. In cases where the half-amplitude region comprised multiple non-contiguous frequency intervals, only the intervals below half-amplitude were included in the width calculation; intervening frequencies that did not fall below half-amplitude were excluded.

4.4.1. Cosine similarity analysis

The pairwise similarity of entrainment threshold curves for different PCs was assessed using the cosine similarity c_{ij},

$$c_{ij} = \frac{E_i(f) \cdot E_j(f)}{||E_i(f)||||E_j(f)||}, \tag{4.4}$$

where i and j index the threshold curves of PCs in a population. We conducted this analysis by separating whole-hand PC populations into PC subpopulations P_k located within different distance ranges from the stimulus CL, where $k = 0, 1, ..., K$ indexes the distance range; P_0 contained all N_0 PCs located within 10 mm of the CL. For $k > 0$, P_k contained all N_k PCs located at distances d_k from the CL satisfying $(20(k-1)+10) \leq d_k < (20k+10)$ mm. Distances on the 2D hand surface were computed from the LDV geometry data using Djikstra's algorithm. We computed the mean cosine similarity σ_k between all PC threshold curves in P_0 and all PC threshold curves in P_k as

$$\sigma_k = \frac{1}{N_0 N_k} \sum_{i=1}^{N_0} \sum_{j=1}^{N_k} c_{ij}. \tag{4.5}$$

We computed the mean pairwise cosine similarity σ_0 between PC threshold curves in P_0 as

$$\sigma_0 = \frac{2}{N_0(N_0-1)} \sum_{i=1}^{N_0} \sum_{j=i+1}^{N_0} c_{ij}. \tag{4.6}$$

4.5. PC population spiking activity analysis

Efficient encoding hypotheses posit that neural sensory circuitry should minimize redundancy [43,44]. We assessed encoding efficiency by analysing mean firing rates and spike timing, both of which are salient to tactile encoding [63–65]. To this end, we assembled a diverse set of stimuli encompassing commonly occurring tactile signals based on prior studies [41,42]. The stimulus set contained 60 sinusoidal, 117 diharmonic and 50 bandpass-filtered noise stimuli that varied in amplitude and frequency parameters (see electronic supplementary material, tables S1–S3). We obtained spike trains evoked in whole-hand PC populations for each stimulus (n = 227), CL (n = 4) and participant (n = 4 or n = 7 depending on the CL).

To assess the redundancy in spiking responses of remotely located PCs, we constructed PC subpopulations P^r located within increasing distances $d_r = 20r$ mm from the CL. The subpopulations formed a nested array of sets, $P^1 \subset P^2 \subset \cdots \subset P^R$, successively encompassing larger numbers of PCs, N^r, where $N^r = N^{r-1} + \Delta N^r$. We analysed spiking responses from each subpopulation using PCA, ISI information entropy and spike train correlations.

4.5.1. Firing rate latent dimensionality analysis

To assess the latent dimensionality of spiking activity from each subpopulation r, PCA was performed on the matrix of time-averaged firing rates M^r_{mn}, where m indexed PCs and n indexed the stimuli. Firing rates were computed as the average spike rate over the entire duration of each stimulus. The data matrix M^r_{mn} was standardized across stimuli (zero-mean and unit standard deviation). To assess the latent dimensionality of the subpopulation firing rates, we computed the minimum number $B(r)$ of principal components that captured at least 99% of the variance (figure 4A). A higher value of $B(r)$ indicated greater firing rate heterogeneity in subpopulation r.

4.5.2. Interspike interval information entropy analysis

We computed ISIs from spike trains $\mathbf{s}^n_m$ evoked in each PC m by each stimulus n. From these data, we computed normalized ISI histograms for each PC subpopulation P^r. In the main results (figure 4B), the histogram bin size was $\Delta t = 1$ ms because PCs encode touch information with millisecond precision [42]. We obtained similar results for values of Δt between 0.5 and 2 ms (electronic supplementary material, fig. S13A–G). We let p^r_q be the probability of an ISI t from P^r falling in the range $t_q \leq t < t_{q+1}$, where $t_q = q\,\Delta t$. We assessed information in spike timing by computing the Shannon information (entropy) $H(r)$, given by

$$H(r) = -\sum_{q=1}^{Q} p^r_q \log_2(p^r_q). \tag{4.7}$$

We also applied the same analysis to individual stimuli (figure 4D and electronic supplementary material, fig. S12). Higher ISI entropy values $H(r)$ indicated more information and less redundancy in spike timing activity.

4.5.3. Spike train correlation analysis

We computed spike train correlations [66–68] using binned spike train vectors with bin width $\Delta t = 1$ ms (Python package, Elephant [69]) (figure 4C). We obtained similar results for values of Δt between 0.5 and 2 ms (electronic supplementary material, fig. S13H–N). For each stimulus n and PC subpopulation P^r, we assessed pairwise spike train correlations by computing Pearson correlation coefficients $c^n_{ij}(r)$ between each pair of binned spike trains $\mathbf{s}^n_i$ and $\mathbf{s}^n_j$, where i and j index PCs in P^r. We computed the mean spike train correlation $c(r)$ for each subpopulation P^r using

$$c(r) = \frac{2}{M(M-1)N} \sum_{n=1}^{N} \sum_{i=1}^{M} \sum_{j=i+1}^{M} |c^n_{ij}(r)|, \tag{4.8}$$

where M is the number of PCs in a subpopulation P^r and N is the number of stimuli. Lower spike train correlations indicated less redundancy within population spike timing activity. By contrast to the ISI entropy analysis, spike train correlations took into account the relative differences in spike times between different PCs.

Ethics. All participants gave their informed, written consent prior to the data collection. The study was approved by the Human Subjects Committee of the University of California, Santa Barbara (Protocol Number 9-18-0676).

Data accessibility. The data and code that support the findings of this study are available on Zenodo [70].

Supplementary material is available online [71].

Declaration of AI use. We have not used AI-assisted technologies in creating this article.

Authors' contributions. N.T.: conceptualization, data curation, formal analysis, methodology, software, validation, visualization, writing—original draft, writing—review and editing; G.R.: conceptualization, data curation, methodology, software, validation, visualization, writing—original draft, writing—review and editing; B.D.: investigation, methodology, software; Y.S.: investigation, methodology; H.S.: conceptualization, methodology, project administration, supervision, writing—original draft, writing—review and editing; Y.V.: conceptualization, funding acquisition, investigation, methodology, project administration, supervision, writing—original draft, writing—review and editing.

All authors gave final approval for publication and agreed to be held accountable for the work performed therein.

Conflict of interest declaration. We declare we have no competing interests.

Funding. This research was supported by National Science Foundation award 1751348 to Y.V. and Leverhulme Trust research project grant RPG-2022-031 to H.P.S. N.T. was supported by a Link Foundation Modeling, Simulation and Training Fellowship and a UC Santa Barbara Graduate Opportunity Fellowship.

Acknowledgements. We thank Benoit Delhaye for feedback and Polytec Inc. for the use of a vibrometry system.

References

1. Gibson JJ. 1966 *The senses considered as perceptual systems*. Boston, MA: Houghton Mifflin Co.
2. Moore TJ. 1970 A survey of the mechanical characteristics of skin and tissue in response to vibratory stimulation. *IEEE Trans. Man-Machine Syst.* **11**, 79–84. (doi:10.1109/TMMS.1970.299966)

3. Andrews JW, Adams MJ, Montenegro-Johnson TD. 2020 A universal scaling law of mammalian touch. *Sci. Adv.* **6**, eabb6912. (doi:10.1126/sciadv.abb6912)
4. Pubols BH. 1987 Effect of mechanical stimulus spread across glabrous skin of raccoon and squirrel monkey hand on tactile primary afferent fiber discharge. *Somatosens. Res.* **4**, 273–308. (doi:10.3109/07367228709144611)
5. Bensmaïa SJ, Hollins M. 2003 The vibrations of texture. *Somatosens. Mot. Res.* **20**, 33–43. (doi:10.1080/0899022031000083825)
6. Delhaye B, Hayward V, Lefèvre P, Thonnard JL. 2012 Texture-induced vibrations in the forearm during tactile exploration. *Front. Behav. Neurosci.* **6**, 37. (doi:10.3389/fnbeh.2012.00037)
7. Johansson RS, Flanagan JR. 2009 Coding and use of tactile signals from the fingertips in object manipulation tasks. *Nat. Rev. Neurosci.* **10**, 345–359. (doi:10.1038/nrn2621)
8. Miller LE, Montroni L, Koun E, Salemme R, Hayward V, Farnè A. 2018 Sensing with tools extends somatosensory processing beyond the body. *Nature* **561**, 239–242. (doi:10.1038/s41586-018-0460-0)
9. Manfredi LR, Saal HP, Brown KJ, Zielinski MC, Dammann JF III, Polashock VS, Bensmaia SJ. 2014 Natural scenes in tactile texture. *J. Neurophysiol.* **111**, 1792–1802. (doi:10.1152/jn.00680.2013)
10. Shao Y, Hayward V, Visell Y. 2016 Spatial patterns of cutaneous vibration during whole-hand haptic interactions. *Proc. Natl Acad. Sci. USA* **113**, 4188–4193. (doi:10.1073/pnas.1520866113)
11. Manfredi LR, Baker AT, Elias DO, Dammann JF, Zielinski MC, Polashock VS, Bensmaia SJ. 2012 The effect of surface wave propagation on neural responses to vibration in primate glabrous skin. *PLoS One* **7**, e31203. (doi:10.1371/journal.pone.0031203)
12. Corniani G, Casal MA, Panzeri S, Saal HP. 2022 Population coding strategies in human tactile afferents. *PLoS Comput. Biol.* **18**, e1010763. (doi:10.1371/journal.pcbi.1010763)
13. Tummala N, Shao Y, Visell Y. 2023 Spatiotemporal organization of touch information in tactile neuron population responses. In *2023 IEEE World Haptics Conf.*, Delft, Netherlands, pp. 183–189. Delft, Netherlands: IEEE. (doi:10.1109/WHC56415.2023.10224467)
14. Thakur PH, Fitzgerald PJ, Hsiao SS. 2012 Second-order receptive fields reveal multidigit interactions in area 3b of the macaque monkey. *J. Neurophysiol.* **108**, 243–262. (doi:10.1152/jn.01022.2010)
15. Muret D, Root V, Kieliba P, Clode D, Makin TR. 2022 Beyond body maps: information content of specific body parts is distributed across the somatosensory homunculus. *Cell Rep.* **38**, 110523. (doi:10.1016/j.celrep.2022.110523)
16. Libouton X, Barbier O, Berger Y, Plaghki L, Thonnard JL. 2012 Tactile roughness discrimination of the finger pad relies primarily on vibration sensitive afferents not necessarily located in the hand. *Behav. Brain Res.* **229**, 273–279. (doi:10.1016/j.bbr.2012.01.018)
17. Nagi SS, McIntyre S, Ng KKW, Mahns DA, Birznieks I, Vickery RM. 2024 Contribution of remote pacinian corpuscles to flutter-range frequency discrimination in humans. *Sci. Rep.* **14**, 27943. (doi:10.1038/s41598-024-79693-5)
18. Verrillo RT, Gescheider GA, Calman BG, Van Doren CL. 1983 Vibrotactile masking: effects of oneand two-site stimulation. *Percept. Psychophys.* **33**, 379–387. (doi:10.3758/BF03205886)
19. Gilson RD. 1969 Vibrotactile masking: some spatial and temporal aspects. *Percept. Psychophys.* **5**, 176–180. (doi:10.3758/BF03209553)
20. Dempsey-Jones H, Harrar V, Oliver J, Johansen-Berg H, Spence C, Makin TR. 2016 Transfer of tactile perceptual learning to untrained neighboring fingers reflects natural use relationships. *J. Neurophysiol.* **115**, 1088–1097. (doi:10.1152/jn.00181.2015)
21. Hunt CC, McIntyre AK. 1960 Characteristics of responses from receptors from the flexor longus digitorum muscle and the adjoining interosseous region of the cat. *J. Physiol.* **153**, 74–87. (doi:10.1113/jphysiol.1960.sp006519)
22. Turecek J, Ginty DD. 2024 Coding of self and environment by pacinian neurons in freely moving animals. *Neuron* **112**, 3267–3277. (doi:10.1016/j.neuron.2024.07.008)
23. Gregory JE, McIntyre AK, Proske U. 1986 Vibration-evoked responses from lamellated corpuscles in the legs of kangaroos. *Exp. Brain Res.* **62**, 648–653. (doi:10.1007/BF00236045)
24. Bouley DM, Alarcón CN, Hildebrandt T, O'Connell-Rodwell CE. 2007 The distribution, density and three-dimensional histomorphology of pacinian corpuscles in the foot of the Asian elephant (*Elephas maximus*) and their potential role in seismic communication. *J. Anat.* **211**, 428–435. (doi:10.1111/j.1469-7580.2007.00792.x)
25. Brisben AJ, Hsiao SS, Johnson KO. 1999 Detection of vibration transmitted through an object grasped in the hand. *J. Neurophysiol.* **81**, 1548–1558. (doi:10.1152/jn.1999.81.4.1548)
26. Dandu B, Shao Y, Visell Y. 2020 Rendering spatiotemporal haptic effects via the physics of waves in the skin. *IEEE Trans. Haptics* **14**, 347–358. (doi:10.1109/TOH.2020.3029768)
27. Rongala UB, Seyfarth A, Hayward V, Jörntell H. 2024 The import of skin tissue dynamics in tactile sensing. *Cell Rep. Phys. Sci.* **5**, 101943. (doi:10.1016/j.xcrp.2024.101943)
28. Sato M. 1961 Response of pacinian corpuscles to sinusoidal vibration. *J. Physiol.* **159**, 391–409. (doi:10.1113/jphysiol.1961.sp006817)
29. Talbot WH, Darian-Smith I, Kornhuber HH, Mountcastle VB. 1968 The sense of flutter-vibration: comparison of the human capacity with response patterns of mechanoreceptive afferents from the monkey hand. *J. Neurophysiol.* **31**, 301–334. (doi:10.1152/jn.1968.31.2.301)
30. Johansson RS, Landström U, Landström R. 1982 Responses of mechanoreceptive afferent units in the glabrous skin of the human hand to sinusoidal skin displacements. *Brain Res.* **244**, 17–25. (doi:10.1016/0006-8993(82)90899-X)
31. Bolanowski SJ, Zwislocki JJ. 1984 Intensity and frequency characteristics of pacinian corpuscles. I. Action potentials. *J. Neurophysiol.* **51**, 793–811. (doi:10.1152/jn.1984.51.4.793)
32. Bell J, Bolanowski S, Holmes MH. 1994 The structure and function of pacinian corpuscles: a review. *Prog. Neurobiol.* **42**, 79–128. (doi:10.1016/0301-0082(94)90022-1)
33. Deflorio D, Di Luca M, Wing AM. 2022 Skin and mechanoreceptor contribution to tactile input for perception: a review of simulation models. *Front. Hum. Neurosci.* **16**, 862344. (doi:10.3389/fnhum.2022.862344)
34. Wiertlewski M, Hayward V. 2012 Mechanical behavior of the fingertip in the range of frequencies and displacements relevant to touch. *J. Biomech.* **45**, 1869–1874. (doi:10.1016/j.jbiomech.2012.05.045)
35. Fradet C, Manfredi LR, Bensmaia S, Hayward V. 2017 Fingertip skin as a linear medium for wave propagation. In *2017 IEEE World Haptics Conf. (WHC)*, Munich, Germany, pp. 507–510. (doi:10.1109/WHC.2017.7989953)
36. Tummala N, Reardon G, Fani S, Goetz D, Bianchi M, Visell Y. 2024 SkinSource: a data-driven toolbox for predicting touch-elicited vibrations in the upper limb. In *2024 IEEE World Haptics Conf.*, Long Beach, CA, USA, pp. 53–60. Long Beach, CA, USA: IEEE. (doi:10.1109/HAPTICS59260.2024.10520852)
37. Hespanha JP. 2018 *Linear systems theory*. Princeton, NJ: Princeton University Press. (doi:10.2307/j.ctvc772kp)
38. Saal HP, Delhaye BP, Rayhaun BC, Bensmaia SJ. 2017 Simulating tactile signals from the whole hand with millisecond precision. *Proc. Natl Acad. Sci. USA* **114**, 5693–5702. (doi:10.1073/pnas.1704856114)
39. Johansson RS, Vallbo AB. 1979 Tactile sensibility in the human hand: relative and absolute densities of four types of mechanoreceptive units in glabrous skin. *J. Physiol.* **286**, 283–300. (doi:10.1113/jphysiol.1979.sp012619)
40. Achenbach JD. 2012 *Wave propagation in elastic solids*. Amsterdam, The Netherlands: Elsevier. (doi:10.1137/1016098)
41. Muniak MA, Ray S, Hsiao SS, Dammann JF, Bensmaia SJ. 2007 The neural coding of stimulus intensity: linking the population response of mechanoreceptive afferents with psychophysical behavior. *J. Neurosci.* **27**, 11687–11699. (doi:10.1523/JNEUROSCI.1486-07.2007)
42. Mackevicius EL, Best MD, Saal HP, Bensmaia SJ. 2012 Millisecond precision spike timing shapes tactile perception. *J. Neurosci.* **32**, 15309–15317. (doi:10.1523/JNEUROSCI.2161-12.2012)

43. Barlow HB. 1961 *Possible principles underlying the transformations of sensory messages*, (ed. WA Rosenblith), pp. 217–234. Cambridge, MA: The MIT Press. (doi:10.7551/mitpress/9780262518420.003.0013)
44. Atick JJ. 1992 Could information theory provide an ecological theory of sensory processing? *Netw. Comput. Neural Syst.* **3**, 213–251. (doi:10.1088/0954-898X_3_2_009)
45. Morley JW, Hawken MJ, Burge PD. 1988 Vibratory detection thresholds following a digital nerve lesion. *Exp. Brain Res.* **72**, 215–218. (doi:10.1007/BF00248520)
46. Mahns DA, Perkins NM, Sahai V, Robinson L, Rowe MJ. 2006 Vibrotactile frequency discrimination in human hairy skin. *J. Neurophysiol.* **95**, 1442–1450. (doi:10.1152/jn.00483.2005)
47. Reardon G, Dandu B, Shao Y, Visell Y. 2023 Shear shock waves mediate haptic holography via focused ultrasound. *Sci. Adv.* **9**, eadf2037. (doi:10.1126/sciadv.adf2037)
48. Stevens SS. 1968 Tactile vibration: change of exponent with frequency. *Percept. Psychophys.* **3**, 223–228. (doi:10.3758/BF03212732)
49. Verrillo RT, Fraioli AJ, Smith RL. 1969 Sensation magnitude of vibrotactile stimuli. *Percept. Psychophys.* **6**, 366–372. (doi:10.3758/BF03212793)
50. von Békésy G. 1955 Human skin perception of traveling waves similar to those on the cochlea. *J. Acoust. Soc. Am.* **27**, 830–841. (doi:10.1121/1.1908050)
51. Saal H, Wang X, Bensmaia S. 2016 Importance of spike timing in touch: an analogy with hearing? *Curr. Opin. Neurobiol.* **40**, 142–149. (doi:10.1016/j.conb.2016.07.013)
52. Bensmaïa S, Hollins M, Yau J. 2005 Vibrotactile intensity and frequency information in the pacinian system: a psychophysical model. *Percept. Psychophys.* **67**, 828–841. (doi:10.3758/BF03193536)
53. Russo FA, Ammirante P, Fels DI. 2012 Vibrotactile discrimination of musical timbre. *J. Exp. Psychol.* **38**, 822–826. (doi:10.1037/a0029046)
54. Johansson R. 1976 Skin mechanoreceptors in the human hand: receptive field characteristics. In *Sensory functions of the skin in primates* (ed. Y Zotterman), pp. 159–170. Pergamon, Turkey: WennerGren Center International Symposium Series. (doi:10.1016/B978-0-08-021208-1.50019-9)
55. Corniani G, Saal HP. 2020 Tactile innervation densities across the whole body. *J. Neurophysiol.* **124**, 1229–1240. (doi:10.1152/jn.00313.2020)
56. Stark B, Carlstedt T, Hallin RG, Risling M. 1998 Distribution of human pacinian corpuscles in the hand. *J. Hand Surg.* **23**, 370–372. (doi:10.1016/S0266-7681(98)80060-0)
57. Germann C, Sutter R, Nanz D. 2021 Novel observations of pacinian corpuscle distribution in the hands and feet based on high-resolution 7-T MRI in healthy volunteers. *Skeletal Radiol.* **50**, 1249–1255. (doi:10.1007/s00256-020-03667-7)
58. Shao Y, Hayward V, Visell Y. 2020 Compression of dynamic tactile information in the human hand. *Sci. Adv.* **6**, eaaz1158. (doi:10.1126/sciadv.aaz1158)
59. Willemet L, Huloux N, Wiertlewski M. 2022 Efficient tactile encoding of object slippage. *Sci. Rep.* **12**, 13192. (doi:10.1038/s41598-022-16938-1)
60. Schafer H, Wells Z, Shao Y, Visell Y. 2017 Transfer properties of touch elicited waves: effect of posture and contact conditions. In *2017 IEEE World Haptics Conf.*, Munich, Germany, pp. 546–551. Munich, Germany: IEEE. (doi:10.1109/WHC.2017.7989960)
61. Liang X, Boppart SA. 2010 Biomechanical properties of *in vivo* human skin from dynamic optical coherence elastography. *IEEE Trans. Biomed. Eng.* **57**, 953–959. (doi:10.1109/TBME.2009.2033464)
62. Timmer J, König M. 1995 On generating power law noise. *Astron. Astrophys.* **300**, 707–710.
63. Harvey MA, Saal HP, Dammann JF 3rd, Bensmaia SJ. 2013 Multiplexing stimulus information through rate and temporal codes in primate somatosensory cortex. *PLoS Biol.* **11**, e1001558. (doi:10.1371/journal.pbio.1001558)
64. Saal HP, Harvey MA, Bensmaia SJ. 2015 Rate and timing of cortical responses driven by separate sensory channels. *eLife* **4**, e10450. (doi:10.7554/eLife.10450)
65. Long KH, Lieber JD, Bensmaia SJ. 2022 Texture is encoded in precise temporal spiking patterns in primate somatosensory cortex. *Nat. Commun.* **13**, 1311. (doi:10.1038/s41467-022-28873-w)
66. Bair W, Zohary E, Newsome WT. 2001 Correlated firing in macaque visual area MT: time scales and relationship to behavior. *J. Neurosci.* **21**, 1676–1697. (doi:10.1523/JNEUROSCI.21-05-01676.2001)
67. Kohn A, Smith MA. 2005 Stimulus dependence of neuronal correlation in primary visual cortex of the macaque. *J. Neurosci.* **25**, 3661–3673. (doi:10.1523/JNEUROSCI.5106-04.2005)
68. Cohen MR, Kohn A. 2011 Measuring and interpreting neuronal correlations. *Nat. Neurosci.* **14**, 811–819. (doi:10.1038/nn.2842)
69. Denker M, Yegenoglu A, Grün S. 2018 Collaborative HPC-enabled workflows on the HBP Collaboratory using the Elephant framework. In *Neuroinformatics*. (doi:10.12751/incf.ni2018.0019)
70. Tummala N, Reardon G, Dandu B, Shao Y, Saal HP, Visell Y. 2025 Biomechanical filtering supports efficient tactile encoding in the human hand (1.1.0) [Data set]. Zenodo. (doi:10.5281/zenodo.17993054)
71. Tummala N, Reardon G, Dandu B, Shao Y, Saal H, Visell Y. 2026 Supplementary material from: Biomechanical filtering supports efficient tactile encoding in the human hand. Figshare. (doi:10.6084/m9.figshare.c.8342004)